

Numerical Investigation of the Fracture Behavior of Tungsten at the Micro Scale

**Christoph Bohnert^{1,2*}, Sabine M. Weygand¹, Nicola J. Schmitt², Ruth Schwaiger²,
Oliver Kraft²**

¹ Faculty of Mechanical Engineering and Mechatronics (MMT), Karlsruhe University of Applied Sciences, Moltkestr. 30,
76133 Karlsruhe (Germany)

² Institute for Applied Materials (IAM), Karlsruhe Institute of Technology (KIT), Hermann-von-Helmholtz-Platz 1,
76344 Eggenstein-Leopoldshafen (Germany)

* Corresponding author: christoph.bohnert2@hs-karlsruhe.de

Abstract Due to its high melting point tungsten has the potential to be used as a structural material in future energy applications. However, one of the challenges is to deal with the brittleness of tungsten at room temperature, where the fracture behavior of polycrystalline tungsten is strongly influenced by the grain structure and texture as well as sample dimensions. The aim of the present work is to numerically analyze the stress field at a notch in a single crystal tungsten micro cantilever. A three dimensional finite element model is presented representing the microstructure of the cantilever which is deflected by a nanoindentation device. The study addresses experimental shortcomings as, for instance, in the experimental setup pure mode I cannot be realized. Due to friction between indenter and microbeam, lateral forces arise and have an impact directly on the stress field at the notch. The FE model is used to study the influence of the friction coefficient on the lateral forces and on the stress intensity factor. The simulations reveal that with rising friction coefficient the lateral force increasing linearly and the stress intensity factor decreases.

Keywords Micro Cantilever, Single Tungsten Crystal, Fracture Toughness, FE Model, Crystal Plasticity

1. Introduction

Tungsten – a material with many outstanding advantages and features – has been mainly used in the light engineering industry as a functional material. Owing to its high melting point, tungsten may be used in the future as a significant structural-material in energy applications. Improvement of the fracture toughness represents one of the challenges due to the brittle-to-ductile transition of tungsten above the room temperature.

Several fracture studies have been already performed on macro specimens. Rupp et al. [1] as well as Gludovatz et al. [2] found a strong influence of the microstructure on the fracture morphology and toughness as well as on the brittle-to-ductile transition temperature in polycrystalline tungsten. The grain structure and texture has namely a decisive influence on the dominating failure mechanisms and on the resulting fracture toughness. In order to consider ways of increasing the fracture toughness, it is therefore necessary to understand the entire complexity of the mechanisms. Gumbsch et al. [3] investigated the fracture toughness of tungsten single crystals with different crystal orientation. They identified fracture toughness values varying from 6.2 to 20.2 MPa m^{1/2} for the {100} and {110} cleavage planes at different crack front directions. However, fracture studies using micro specimens are very rare. Wurster et. al. [4-5] performed fracture experiments on tungsten single crystal notched micrometer-sized cantilevers.

In the present work the fracture behavior of single tungsten crystals is numerically analyzed for micro scale samples. This is related to an ongoing experimental study on single crystal tungsten microbeams with the focus on crack initiation and crack growth performed by N. Schmitt [6]. In the experimental work notched cantilevers with a height of 55 μm and a width of 28 μm are manufactured and bend by a nanoindenter. Experimental shortcomings are for instance the deviation from ASTM standard geometry and the deviation from the pure mode I. To support and complement the experiments a finite element model of the microbending test is presented in the present paper. It is applied to compute the stress intensity factor K for the present nonstandard specimen geometry. Furthermore, it is used to analyze the influence of lateral forces (due to friction between indenter and microbeam) on the stress intensity factor and to evaluate different nanoindenter geometries.

2. Modelling

2.1 Geometry

To determine the fracture toughness standardized test geometries are mainly used in accordance with ASTM standards, such as the three-point bending test (3PB) or the compact tensile specimen (CT). However, it should be noted that the stress intensity factor K depends on the specimen geometry as well as the respective crack opening mode. Mode I, the opening mode, represent the most important type of crack opening which is characterized by a tensile stress normal to the crack plane. By considering the critical case under mode I and plane strain conditions, the fracture toughness K_{Ic} can be determined at the beginning of the crack extension according to ASTM standard E399-90 [7]. As in the present work fracture is studied at the micro scale, the rules of the ASTM standard do not hold anymore. Therefore a new geometry had to be developed.

To ensure efficient and rapid manufacturing of the tungsten micro cantilevers, a geometry based on the specifications of the standard ASTM sample is chosen. This geometry is shown in Fig. 1. Its width W is 55 μm with a thickness B of 28 μm and a crack length a of 15 μm . The proportions between width W , thickness B and crack length a are identical to the ones of the standard ASTM samples. This is to ensure the relationship between macro and micro scale. The developed sample geometry allows the analysis of micro-specific effects of notches and multiaxial load conditions. Due to the miniaturized geometry size-effects occur, which is caused by proportions of the plastic zone in front of the crack tip as well as the changed sample ratio of surface to volume. Therefore it is not possible to transfer known macroscopic material properties into the micro scale. Based on this fact an experimental programme is carried out (N. J. Schmitt) and combined with a numerical analysis to determine the necessary characteristics at the micro scale (100 to 300 μm).

2.2 Finite element model

The notched micro cantilever is represented by a three dimensional finite element (FE) model shown in Fig. 2. Due to the symmetry only one half of the specimen is modeled and meshed with 8-node brick elements with linear function (C3D8). Besides the symmetry conditions fixed boundary conditions are applied at the right end (see Fig. 2). The indenter is modeled as rigid body. Its movement in z-direction is prescribed while the indenter cannot move in x-direction (lateral direction) and in y-direction. The developed model is implemented in the finite element code ABAQUS [8]. In the first simulations purely linear elasticity is applied as constitutive law. In later simulations crystal plasticity is added.

2.3 Crystal plasticity as constitutive law

As plastic behavior can be observed at the crack tip, crystal plasticity is implemented in the FE model as a plastic constitutive law as it allows specifying the crystal orientation of the tungsten single crystal. The theory of crystal plasticity is based on the assumption that plastic deformation (crystalline slip) results as the sum of all activated slip systems. Schmid (1931) [9] found, that the resolved shear stress onto a crystallographic plane leads to plastic slip, if stress reaches a critical value. This resolved stress on a slip system, which is also called the Schmid stress is assumed for this constitutive law as the only driving force for slip. The exact theory was formulated by Hill and Rice (1972) [10]. First FE studies of single crystals have been carried by Peirce, Asaro and Needleman (1982) [11].

The rate dependent plastic constitutive law was formulated by Asaro [12] and written by Huang [13] as a user-material subroutine UMAT. This UMAT is used in the presented simulations. It allows investigating the influence of the crystal orientation on the stress intensity factor. Two slip system families are taken into account, namely the $\{110\}\langle 111\rangle$ and the $\{112\}\langle 111\rangle$.

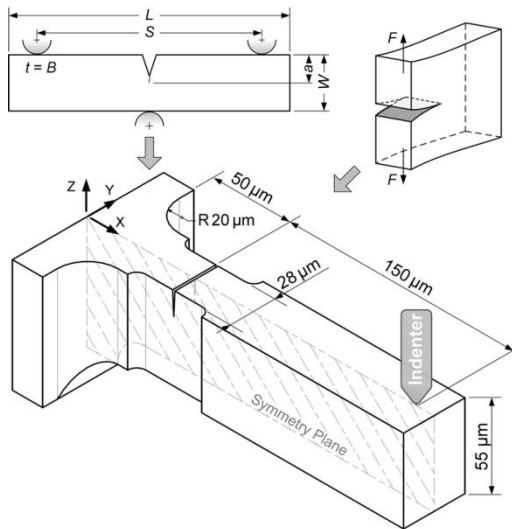


Figure 1. Specimen geometry of the micro cantilever based on single edge notch bending mimicking crack opening mode I.

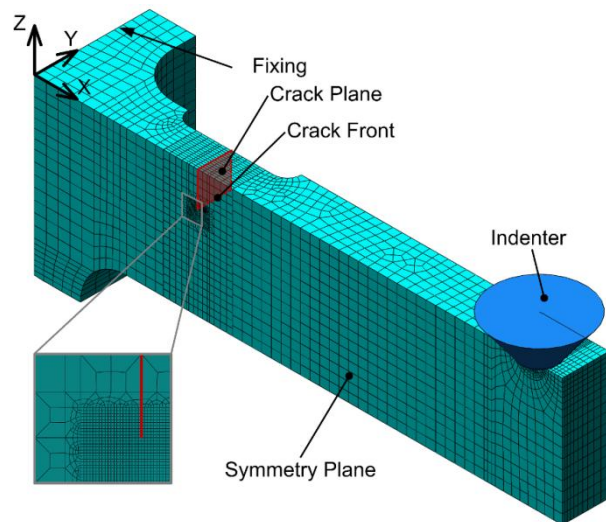


Figure 2. Three-dimensional finite element model of the micro cantilever showing the used mesh and the applied boundary conditions.

The material parameters are fitted to experimental results of Argon and Maloof (1966) [14]. They investigated the mechanical behavior of single tungsten crystals via tensile tests at different orientations. The material parameters were fitted to the $\{112\}$ -tensile orientation. Table 1 summarizes the found material parameters initial hardening modulus h_0 , initial yield stress τ_0 and stage 1 stress τ_s for each slip system family.

Table 1. Estimated material parameters of the two system families

slip system	$\{110\}\langle 111\rangle$	$\{112\}\langle 111\rangle$
h_0 [MPa]	3700	3800
τ_0 [MPa]	140	145
τ_s [MPa]	385	400

3. Results and Discussion

Elastic study of the bending of the micro cantilever

In the fracture experiment an indenter moves with a speed of 20 nm per second in negative z-direction (see Fig. 2). Its reaction force (named $RF3$) is measured together with the prescribed displacement u in z-direction. As the crack opens during bending, the cantilever moves relative to the indenter and friction occurs resulting in a lateral force called $RF1$ and in a deviation from pure mode I. Its size and effect on the stress field around the crack tip are unknown and experimentally hardly accessible. To clarify the influence of the lateral forces, the purely elastic model presented in section 2 was applied to simulate displacement controlled bending of the micro cantilever. As the friction coefficients μ are not available, it was varied between 0 and 0.4. Additionally, different geometries of the indenter tip were applied in the FE simulations:

1. Indenter R2 (0.2 μm)
2. Indenter R10 (0.2 and 0.5 μm)
3. Wedge R10 (0.5 μm)
4. Concentrated Force
5. Pressure

Indenter R2 and indenter R10 are simplified axisymmetric simplifications of the common Berkovich tip; contrary to the common tip radius of a Berkovich tip of less than 20 nm, the elected tip radiuses are 2 and 10 μm . The values in parentheses correspond to the mesh size at the contact. To demonstrate the effect of an increased contact surface a wedge tip was chosen resulting in line loading instead of point loading.

Beside these displacement controlled simulations load controlled bending simulations are also performed where concentrated point loads (in z- and y-direction) are applied on a surface in place of contact conditions (referred as concentrated force). The advantage of this load condition is that normal (*RF3*) and lateral force (*RF1*) can be chosen independently. The concentrated point load has also been replaced with a surface pressure normal to beam surface (referred as pressure).

As expected the indenter penetration strongly depends on the indenter tip geometry. Fig. 3 shows the computed displacement of the material beneath and near the indenter in the z-direction for the three different indenter tip geometries (Indenter R2, Indenter R10 and Wedge R10) and the force controlled loading (Concentrated Force / Pressure) at the same indenter tip depth of 11.1 μm with a friction coefficient of $\mu = 0.2$. It becomes apparent that tips with a small radius lead to a more localized deformation beneath the indenter tip. On the one hand, the difference between the displacement of the indenter tip (experimentally easy measurable) and the displacement at the beam surface is relative large. This causes an indenter dependent error in the displacement measurement. On the other hand the indentation with a small tip radius ($R = 2 \mu\text{m}$) results in a larger lateral force *RF1* in relation to the normal force *RF3*. With a wedge indentation the deformation is more homogeneous. Thus, in the experimental setup with the wedge tip the measured displacement is more accurate.

Several simulations were performed to evaluate the influence of the lateral forces on the stress field at the crack tip. In linear elastic fracture mechanics (LEFM) the stress intensity factor *K* characterizes this stress field. The critical stress intensity factor K_{Ic} , which leads to crack growth is also called fracture toughness.

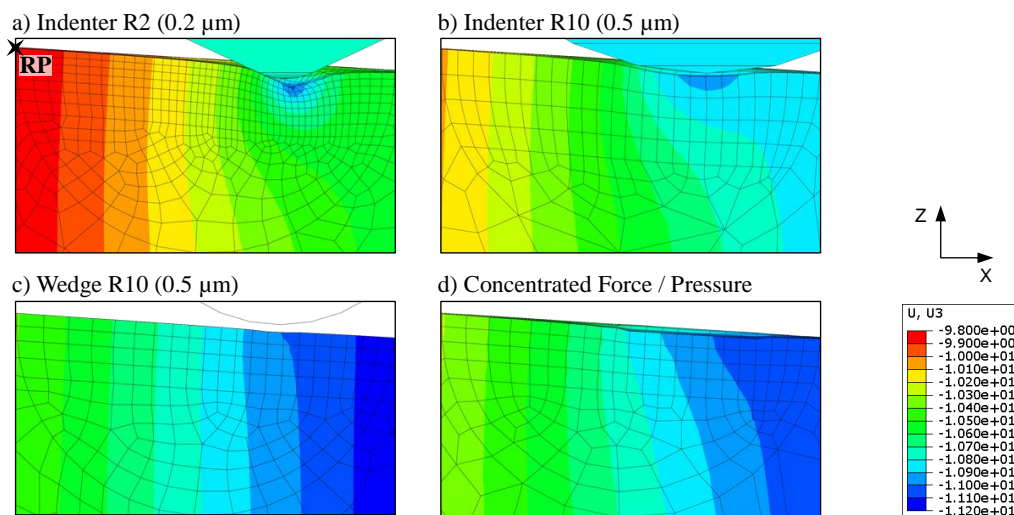


Figure 3. Displacement in z-direction of the material in the symmetry plane in the vicinity of the indenter for different indenter tip geometries at the same indenter tip displacement. The indenter with $R = 2 \mu\text{m}$ shows in a) a substantially greater penetration compared to $R = 10 \mu\text{m}$ in b), to the wedge tip in c) and the concentrated force and pressure in d).

Another fracture parameter is the J -integral which characterizes the strain energy release rate and which can be calculated in the linear elastic range for mode I with

$$J_{Ic} = G_{Ic} = K_{Ic}^2 \left(\frac{1-\nu^2}{E} \right) \quad (1)$$

from the fracture toughness K_{Ic} . G_{Ic} corresponds to the critical strain energy release rate, ν is the Poisson's ratio of 0.28 and E is the elastic modulus of tungsten with 410 GPa.

Applying the purely elastic FE model the stress intensity factor for each mode (I, II or III) as well as the J -integral was calculated along the crack front for various indenter tip geometries. Additionally a parameter study with a friction coefficient varying from 0 to 0.4 was performed. The results are shown in Fig. 4. The J -integral (at an indenter tip displacement of 11.1 μm) is plotted as a function of the ratio of the lateral force to the normal force ($RF1/RF3$).

First it shows that independently of the indenter tip geometry the J -integral decreases linearly with increasing lateral force $RF1$. Furthermore, it is apparent that even without friction ($\mu = 0$) a lateral force occurs where the $RF1/RF3$ values vary from 0.25 to 0.44. The lateral force itself increases with increasing friction coefficient. The diagram also reveals the influence of the indenter tip geometry: the more localized the penetration of the indenter, the smaller is the overall bending of the cantilever leading to smaller J values (see Indenter R2 and R10).

Instead of using the indenter tip as reference point for the displacement a different reference point (RP) outside the process zone of the indenter has been selected at the sample surface of the beam with the coordinates of 10 μm in negative x -direction at the crack tip. This time the J -integrals are compared at 10 μm displacement of this newly selected reference point (Fig. 3 a)). Fig. 5 shows the computed J -integrals as a function of the lateral to normal load for various indenters. In this way the dependence of the J -integral on the indenter geometry is eliminated and the J -integral is only determined by the ratio of the lateral to normal force. The deviation of the J values for the same indenter tip displacement can reach up to 12%.

In a mesh study the local mesh refinement at the contact surfaces from 0.5 to 0.2 μm indicates no effect on the J -integral.

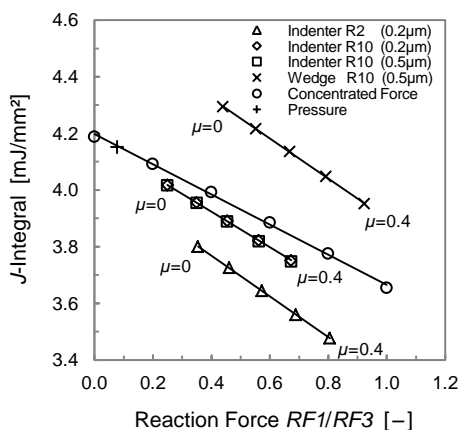


Figure 4. J -integral as a function of the ratio of lateral to normal load at 11.1 μm indenter tip displacement revealing an influence of the indenter geometry.

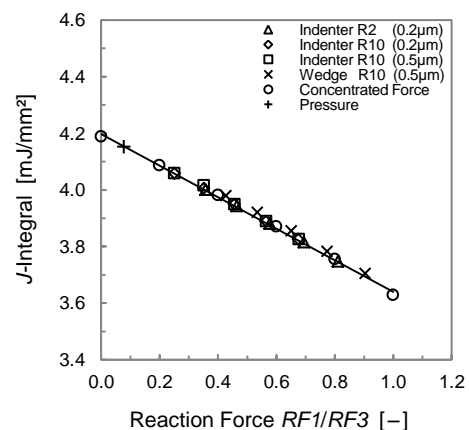


Figure 5. J -integral as a function of the ratio of lateral to normal load at 10 μm displacement of a chosen reference point (RP).

As already mentioned a lateral force always occurs during bending. Therefore, we analyze the mixed mode.

On the basis of the LEFM, stress intensity factors of the respective modes with K_I , K_{II} and K_{III} can be calculated and evaluated. Mathematically, the K factors can be calculated numerically very well within the finite element code. Fig. 6 shows the resulting three K factors for different indenter tip geometries and varying friction. It becomes clear that mode I is the dominant mode. However, its value slightly decreases with increasing lateral force. The K_{II} value is about 6% of K_I and its value slightly rises with increasing lateral force. Mode III is not present. Based on the large differences between the values of K_I to K_{II} we can assume pure mode I.

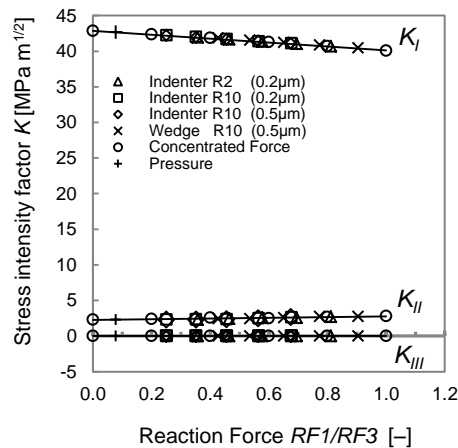


Figure 6. Stress intensity factors for mode I, II and III as a function of the ratio of lateral to normal load at 10 μm reference point displacement.

Simulation of the bending of the micro cantilever with crystal plasticity

As described in Section 2 the elastic FE model was extended by crystal plasticity. This allows to take into account the orientation of the single crystal and to evaluate the plastic deformation ahead of the crack front. The crystal plasticity model was applied to simulate the bending of a beam without (CF0.0) and with a ratio of the lateral force to the normal force of 0.4 (CF0.4). Instead of modeling the contact between indenter and beam explicitly the simulation is performed load controlled as concentrated force in normal and lateral load (see concentrated force).

The simulated beams are aligned in such a way that the $\{110\}\langle 0\bar{1}1\rangle$ -crack system lies in the loading direction.

Results of the simulations are, besides stress and strain fields, the force-displacement curve, the evolution of the J -integral at the crack front and the slip activities. Fig. 7 illustrates the resulting force-displacement curves for the two cases with and without lateral force. Is a lateral force $RF1$ present, the normal force $RF3$ is increased. The difference in force results from the interplay of material deformation and material accumulation in front of the indenter (during bending).

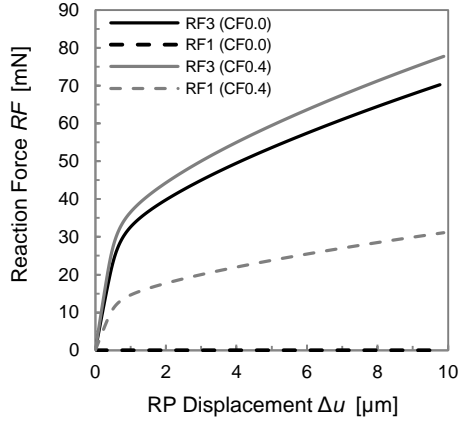


Figure 7. Characteristic force-displacement curve of the normal ($RF3$) and the lateral force ($RF1$) under load of a single tungsten crystal with $\{011\}\langle 0\bar{1}1\rangle$ -crack system, exemplary for the ratio $RF1/RF3 = 0$ (CF0.0) and $RF1/RF3 = 0.4$ (CF0.4).

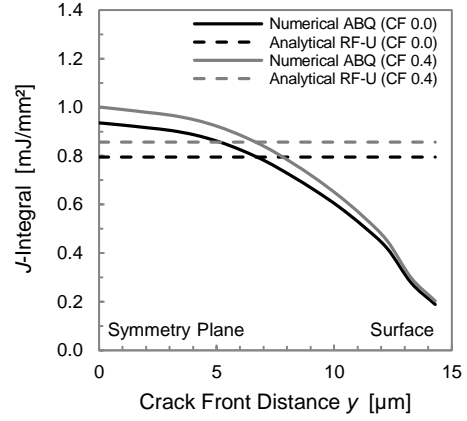


Figure 8. Course of the J -integral along the crack front, from the symmetry plane up to surface., exemplary for the ratio $RF1/RF3 = 0$ (CF0.0) and $RF1/RF3 = 0.4$ (CF0.4) at $10 \mu\text{m}$ reference point displacement.

We obtained the J -integral in two ways: first with the analytical relations of the standard ASTM E1820 [15] using the force-displacement curve (commonly applied in fracture experiments) and secondly numerically.

J consists of an elastic J_{el} and plastic J_{pl} contribution. According to [15] the J -integral is calculated with:

$$J = J_{el} + J_{pl} = \frac{K^2(1-\nu^2)}{E} + \frac{\eta A_{pl}}{B b_o}, \quad (2)$$

where A_{pl} defines the plastic work of the applied load, B the specimen thickness and b_o is defined by the difference between the width W and the initial crack length a_o . The non-dimensional η describes the effect of plastic work normalized by the ligament area. For deep notch specimens, standard [7] and [15] prescribe η by the following definition:

$$\eta = 2 \quad , \text{when } 0.45 \leq \frac{a}{W} \leq 0.55 \quad (3)$$

With an investigated a/W -relation of 0.27, the standard approach of η is just an approximation. Based on a numerical fit to a number of different FEM solutions, Nevalainen and Wallin [16] obtained a crack length dependent correlation of η :

$$\begin{aligned} \eta &= 13.818 \cdot \frac{a}{W} - 25.124 \cdot \left(\frac{a}{W}\right)^2 \quad , \text{when } 0 < \frac{a}{W} \leq 0.274 \\ \eta &= 1.859 + \frac{0.03}{1 - \frac{a}{W}} \quad , \text{when } 0.274 < \frac{a}{W} \leq 0.9 \end{aligned} \quad (4)$$

According to [16] and with a geometry relation of $a/W = 0.27$, η can be determined from Eq. (4) to be 1.9 leading to a J of 0.80 mJ/mm^2 at an reference point displacement of $10 \mu\text{m}$ when no lateral force is present. In case of $RF1/RF3 = 0.4$ the J increases to 0.86 mJ/mm^2 .

In the numerical approach the J -integral can be determined along the crack front. Its course is given in Fig. 8. As expected, the maximum J value occurs at the symmetry plane in the state of plane strain, the so-called critical condition. Here, it is also expected that crack initiation starts with subsequent crack propagations.

Fig. 8 shows furthermore, that the numerical J values in the center of the specimen (symmetry plane) are larger and at the surface smaller than the analytical values. A comparison of the analytical solution with $J_{an} = 0.71 \text{ mJ/mm}^2$ and the average numerical solution with $J_{num} = 0.80 \text{ mJ/mm}^2$ shows a good and plausible approximation.

Thanks to crystal plasticity the activities on various slip systems can be revealed. To get an idea of the size of the zone with slip activities the accumulated shear strain is shown in Fig. 9 in front of the crack tip and at the surface for an indenter displacement of $0.5 \text{ }\mu\text{m}$. As known from the fracture mechanics, the plastic zone is in the symmetry plane due to plane strain smaller than at the surface. The influence of the asymmetric specimen geometry can be also seen. The fixing is located on the left side and the loading takes place on the right side. Here, the load results to $RF3 = 25 \text{ N}$ and to $RF1 = 10 \text{ N}$.

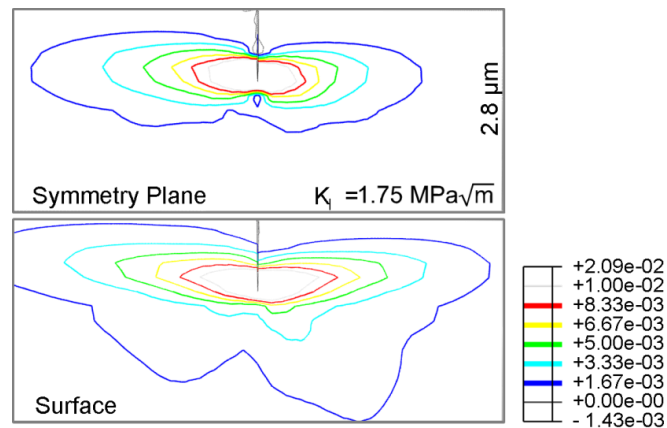


Figure 9. Accumulated shear strain ahead of the crack tip at a indenter displacement of $0.5 \text{ }\mu\text{m}$ for an orientation $\{011\}\langle 0\bar{1}1\rangle$ of the crack system, exemplary details were chosen in the symmetry plane and at the surface.

5. Conclusion

In this paper we presented a three dimensional finite element model of a notched single crystalline tungsten micro cantilever which is deflected in the bending test by a nanoindentation device. The model was applied to study the influence of friction and indenter geometry on the stress field around the crack (notch) characterized by the stress intensity factor K or the J -integral. The results show that with increasing friction coefficient μ the lateral force increases linearly and with it the J -integral decreases linearly. Furthermore, the indenter tip geometry plays an important role. Based on these numerical results following recommendations can be made regarding the experimental setup. To exclude the influence of the indenter tip geometry, the displacement should not be measured at the indenter tip but at a point slightly ahead of the indenter (outside the penetration area). The simulations show that otherwise the error of the J -integral can reach up to 12% (e.g. in case of an axisymmetric Berkovich tip like indenter with a tip radius of $2 \text{ }\mu\text{m}$). If only the displacement of the indenter tip is experimentally accessible, an indenter with a large contact area (e.g. a wedge indenter) is recommended as localized penetration is prevented and the error in J is minimized.

Acknowledgements

The authors would like to thank the Karlsruhe University of Applied Sciences and Karlsruhe Institute of Technology (KIT) for providing the necessary equipment.

The research was financial supported by a fellowship of the “Kooperatives Promotionskolleg: Gefügestrukturanalyse und Prozessbewertung” funded by the Postgraduate Research Grants Programme of Baden-Württemberg (Germany).

References

- [1] D. Rupp, S. M. Weygand, Anisotropic fracture behaviour and brittle-to-ductile transition of polycrystalline tungsten, *Philosophical Magazine*, vol. 90, pp. 4055–4069, 2010.
- [2] B. Gludovatz, S. Wurster, A. Hoffmann, R. Pippan, Fracture toughness of polycrystalline tungsten alloys, *Int. J. of Refrac. Met. and Hard Mat.*, vol. 28, pp. 674–678, 2010.
- [3] P. Gumbsch, Brittle fracture and the brittle-to-ductile transition of tungsten, *J. of Nuclear Materials*, vol. 323, pp. 304–312, 2003.
- [4] S. Wurster, C. Motz, M. Jenko, R. Pippan, Micrometer-Sized Specimen Preparation Based on Ion Slicing Technique, *Advanced Engineering Materials*, vol. 12, pp. 61–64, 2010.
- [5] S. Wurster, C. Motz, R. Pippan, Characterization of the fracture toughness of micro-sized tungsten single crystal notched specimens, *Phil. Mag.*, vol. 92, pp. 1803–1825, 2012.
- [6] N. J. Schmitt, C. Bohnert, C. Eberl, R. Schwaiger, S. M. Weygand, O. Kraft, Investigation of the fracture behavior of tungsten at the micro scale, *ICF13th International Conf. on Fracture*, Beijing, 2013.
- [7] ASTM E399 - 90: Standard test method for plane-strain fracture toughness of metallic materials, *Annual Book of the ASTM Standards*.
- [8] Simulia Dassault Systemes GmbH, Abaqus CAE (Version 6.11), www.3ds.com.
- [9] E. Schmid, Beiträge zur Physik und Metallographie des Magnesiums, *Zeitschr. Elektrochem.*, vol. 37, pp. 447–459, 1931.
- [10] R. Hill, J. R. Rice, Constitutive analysis of elastic-plastic crystals at arbitrary strain, *Journal of the Mechanics and Physics of Solids*, vol. 20, pp. 401–413, 1972.
- [11] D. Peirce, R. J. Asaro, A. Needleman, An analysis of nonuniform and localized deformation in ductile single crystals, *Acta Metallurgica*, vol. 30, pp. 1087–1119, 1982.
- [12] R. J. Asaro, *Micromechanics of Crystals and Polycrystals*, *Advances in Applied Mechanics*, vol. 23, pp. 1–115, 1983.
- [13] Y. Huang, A user-material subroutine incorporating single crystal plasticity in the ABAQUS finite element program, *Mech Report*, 1991.
- [14] A. S. Argon, S. R. Maloof, Plastic deformation of tungsten single crystals at low temperatures, *Acta Metallurgica*, vol. 14, pp. 1449–1462, 1966.
- [15] ASTM E1820 - 01: Standard Test Method for Measurement of Fracture Toughness, *Annual Book of the ASTM Standards*.
- [16] M. Nevalainen, K. Wallin, The effect of crack depth and absolute thickness on fracture toughness of 3 PB specimens, *Proc. ECF10th European Conf. on Fracture*, pp. 997–1006, 1994.